Dispersion effects in fiber optic interferometry

Shellee D. Dyer*
Douglas A. Christensen
University of Utah
Department of Electrical Engineering
Salt Lake City, Utah 84112
E-mail: christen@ee.utah.edu

Abstract. An extended analysis of the effects of uncompensated fiber dispersion on the fringe visibility of a fiber optic interferometer is developed, with particular emphasis on stellar interferometry. Both material and waveguide dispersion for single-mode, polarization-preserving fibers are considered. It is found that dispersion causes the fringe visibility curve to broaden, decrease in contrast, shift its centroid location, and in some cases become asymmetric. It is also shown that when the interferometer is operated at wavelengths near 1300 nm, cancellation of second-order material and waveguide dispersion significantly improves the fringe visibility. The theoretical results are verified experimentally at both 672 nm and 1307 nm using a fiber optic Mach-Zehnder interferometer.
[S0091-3286(97)03809-9]

Subject terms: interferometry; stellar interferometry; fiber optics; dispersion; statistical optics.

Paper 19037 received Mar. 14, 1997; revised manuscript received June 4, 1997; accepted for publication June 5, 1997.

1 Introduction

In the Michelson stellar interferometer, the starlight collected by two or more widely separated telescopes is brought to a central location and combined to form interference fringes.[1] Under ideal conditions, the fringe visibility is equal to the magnitude of the complex degree of coherence γ_{12} of the incident light. Using the Van Cittert-Zernike theorem, the complex degree of coherence can be expressed as the Fourier transform of the spatial intensity distribution of the source.[2]

Conventionally, the light from the telescopes is passed through vacuum or temperature-controlled air tubes, which must be carefully aligned to bring the light to the recombination point.[1] For example, the Center for High Angular Resolution Astronomy (CHARA) is currently constructing an optical array consisting of five 1 m aperture telescopes in a Y-shaped configuration confined within a 400 m diameter circle on Mount Wilson in California.[3] The beam transfer subsystem of the CHARA array consists of both evacuated paths (for optical path length equalization) and environmentally controlled air paths.

The replacement of vacuum and air paths (or portions thereof) with optical fibers has been recently proposed.[4–8] Optical fibers have several advantages, such as requiring fewer alignment-sensitive reflection surfaces, and, after the light is coupled to the fibers, the problems of diffraction, misalignment and optical surface quality are no longer a concern. In addition, the light output from single-mode fibers has nearly perfect spatial coherence, reducing the effects of atmospheric turbulence and other distortions.[6] Optical fibers also greatly simplify the beam recombination process by using directional couplers.[7]

However, optical fibers typically display significantly higher dispersion (i.e., a variation of effective refractive index with wavelength) than air paths, which can adversely affect the performance of the interferometer. For example, one effect of uncompensated dispersion is to reduce the fringe visibility from the ideal value of $|\gamma_{12}|$, increasing the difficulty of accurately determining the intensity distribution of the source. Fiber dispersion does not affect the fringe visibility if the interferometer arms have equal fiber lengths, but in general the light from a star will arrive at an oblique angle Ω with respect to the normal to the plane containing the telescopes, which introduces a relative delay in the signals reaching the telescopes. To achieve zero optical path length difference (OPD), this astrometric delay must be balanced, preferably with extra fiber in the opposite arm of the interferometer, leading to uncompensated fiber dispersion.

To increase the number of photons collected from weak astronomical objects, moderately broadband (25 nm or greater) light is passed through the interferometer. A broadband source can be thought of as a collection of many narrowband sources, each centered at a different wavelength. Due to dispersion, each of these narrowband sources will have a different air path length for zero OPD, and the resultant visibility curve will be the sum of many shifted visibility packets. Thus it is anticipated that the net visibility will be reduced from its ideal value, and spread over a broader range of OPD.

The effects of dispersion in an air-path stellar interferometer have been thoroughly described by Tango.[9] In that study, the fringe visibility was calculated by expanding the frequency-dependent terms of the Wiener-Khinchin theorem using a Taylor series expansion. To extend the analysis to a fiber optic interferometer, waveguide dispersion terms must be included. Reynaud et al. discussed dispersion effects in fiber interferometers in terms of the second-order derivative of the fiber propagation constant, and gave an

*Current affiliation: National Institute of Standards and Technology, 325 Broadway, Boulder, CO 80303.

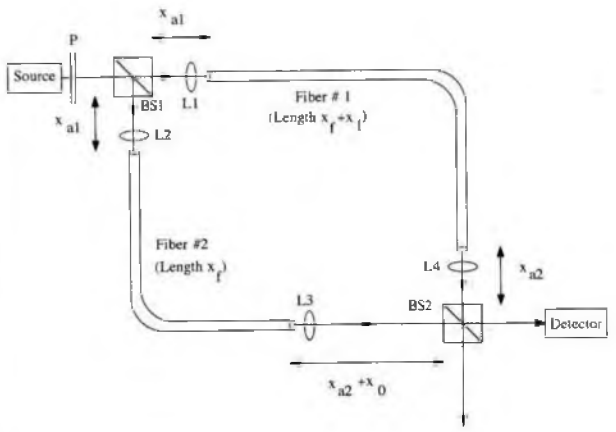

Fig. 1 Mach-Zehnder model for a fiber optic stellar interferometer. The fiber length difference x_1 between the two arms is compensated by the vacuum path length difference x_0: BS, beamsplitter; L, lens; and P, polarizer.

expression for the maximum tolerable fiber-length difference.[10] Coudé du Foresto et al. investigated fiber dispersion effects in double Fourier stellar interferometers by relating the phase curvature of the interferograms to the dispersion parameters of the fiber.[11] They considered dispersion terms up to second order.

In this paper, we present a complete theory that describes the effects of both material and waveguide dispersion on fringe visibility using higher order dispersion terms (up to fifth order is demonstrated). These higher order dispersion terms are particularly important in the near IR, where the second-order dispersion term is near zero. Our development extends the analysis of dispersion effects in an air-path interferometer by Tango.[9] In optical communications using single-mode silica fibers, it is well known that the pulse spread due to waveguide dispersion can cancel the pulse spread due to material dispersion at wavelengths near 1300 nm (Ref. 12). However, it has not yet been determined how the choice of operating wavelength affects fringe visibility in fiber interferometers. In this paper, we show that the visibility can be significantly improved by a judicious choice of mean wavelength. Our theoretical results are compared to experimentally measured visibilities at both visible and IR wavelengths.

2 Theory

2.1 *Analysis*

The fiber optic stellar interferometer is modeled in Fig. 1 as a Mach-Zehnder interferometer consisting of two single-mode fibers of unequal length and a vacuum path in one arm to compensate the unequal lengths. Since polarization rotation has a deleterious effect on fringe visibility, polarization-maintaining (PM) fibers are assumed in this analysis and polarization mode dispersion is therefore neglected. The total OPD can be written as

$$X=\frac{\beta}{k}x_1-x_0, \tag{1}$$

where β is the fiber propagation constant, k is the free space propagation constant, β/k is the effective refractive index of the fiber, x_1 is the difference in length between the two fibers, and x_0 is the length of the compensating vacuum path. Most optical fibers are strongly dispersive and thus the effective refractive index is a function of wavelength. The OPD is then also a function of wavelength and can be written in terms of the spectroscopic wavenumber ($\sigma=\lambda^{-1}$) as $X=X(\sigma)$.

At the output of the interferometer the complex degree of coherence $\gamma(X)$ is given by

$$\gamma(X)=\int_0^\infty \hat{\mathscr{S}}(\sigma)\exp\left[-j2\pi\sigma X(\sigma)\right]\mathrm{d}\sigma, \tag{2}$$

where $\hat{\mathscr{S}}(\sigma)$ is the power spectral density of the source, normalized for unit area.[2] The fringe visibility is given by $V(X)=|\gamma(X)|$.

In the nondispersive case $\gamma(X)$ and $\hat{\mathscr{S}}(\sigma)$ are a Fourier transform pair since $X(\sigma)$ is a constant. For the dispersive case, it is useful to express Eq. (2) as a Fourier transform also. To accomplish this, we use Tango's definition of the mean wavenumber $\bar{\sigma}$ as[9]

$$\bar{\sigma}=\frac{\int_0^\infty \sigma\hat{\mathscr{S}}^2(\sigma)\mathrm{d}\sigma}{\int_0^\infty \hat{\mathscr{S}}^2(\sigma)\mathrm{d}\sigma}. \tag{3}$$

We then expand $\sigma X(\sigma)$ in a Taylor series around the mean wavenumber. Using Eq. (1) for $X(\sigma)$ and letting $s=\sigma-\bar{\sigma}$, the Taylor series expansion of $\sigma X(\sigma)$ can be expressed as[9]

$$\sigma X(\sigma)=\bar{\sigma}X(\bar{\sigma})+(b_1x_1-x_0)s+b_2x_1s^2+b_3x_1s^3+\cdots, \tag{4}$$

where the n'th-order dispersion term is given by

$$b_n=\frac{1}{n!}\frac{\mathrm{d}^n}{\mathrm{d}\sigma^n}\left(\sigma\frac{\beta}{k}\right)\bigg|_{\sigma=\bar{\sigma}}. \tag{5}$$

At this point it is helpful to make several approximations. First, the fiber is assumed to be weakly guiding, which requires that the fiber profile parameter Δ, defined as

$$\Delta=\frac{n_1-n_2}{n_1}, \tag{6}$$

where n_1 and n_2 are the refractive indices of the core and clad, respectively, be much smaller than unity.[13] This approximation is valid for most commercially available single-mode fibers. For a weakly guiding fiber the propagation constant β is approximately given by

$$\beta\approx n_2k(1+b\Delta), \tag{7}$$

where b is the normalized propagation constant.[13] We also assume that the fiber profile parameter Δ is independent of

wavenumber. This is equivalent to assuming that the core and clad have approximately the same material dispersion characteristics.

Substituting Eq. (7) into Eq. (5) with algebraic simplification, the first-order dispersion term b_1 can be expressed as

$$b_1=\left(n_2+\bar{\sigma}\frac{dn_2}{d\bar{\sigma}}\right)+\left(b\Delta n_2+b\Delta\bar{\sigma}\frac{dn_2}{d\bar{\sigma}}+\bar{\sigma}n_2\Delta\frac{db}{d\bar{\sigma}}\right), \quad (8)$$

where $d/d\bar{\sigma}$ is used to represent $d/d\sigma$ evaluated at $\bar{\sigma}$. To further simplify this expression, we note that for all glasses of interest $\sigma dn_2/d\sigma \ll n_2$, and therefore the product of $b\Delta$ with $(\bar{\sigma})(dn_2/d\bar{\sigma})$ can be neglected with respect to the $b\Delta n_2$ term.[13] Making this approximation and rewriting the derivative $db/d\bar{\sigma}$ in terms of the fiber V number, the first-order dispersion coefficient b_1 simplifies to

$$b_1=\left(n_2+\bar{\sigma}\frac{dn_2}{d\bar{\sigma}}\right)+\left[n_2\Delta\frac{d(Vb)}{dV}\right]. \quad (9)$$

The first term of this equation in parentheses is the material dispersion term, while the second bracketed term is the waveguide dispersion term. This expression is proportional by a factor of L/c to the expression for group delay used in optical fiber communications, where L is the total fiber length and c is the vacuum velocity of light.[13]

The second-order dispersion term b_2 is derived by a similar procedure, giving

$$b_2=\frac{1}{2}\left[\left(2\frac{dn_2}{d\bar{\sigma}}+\bar{\sigma}\frac{d^2n_2}{d\bar{\sigma}^2}\right)+\left(n_2\Delta\frac{V}{\bar{\sigma}}\frac{d^2(Vb)}{dV^2}\right)\right], \quad (10)$$

which again is the sum of a material dispersion term and a waveguide dispersion term. The second-order dispersion term b_2 is proportional by a factor of $2L\delta\lambda\sigma^2/c$ to the expression for pulse spread in optical fiber communications, where $\delta\lambda$ is the source spectral width.[12]

The higher order dispersion terms can be derived in a similar fashion. In general, the n'th-order dispersion term is given by

$$b_{n,\mathrm{tot}}=b_{n,\mathrm{mat}}+b_{n,\mathrm{wg}}, \quad (11)$$

where

$$b_{n,\mathrm{mat}}=\frac{1}{n!}\left(n\frac{d^{n-1}n_2}{d\bar{\sigma}^{n-1}}+\bar{\sigma}\frac{d^nn_2}{d\bar{\sigma}^n}\right), \quad (12)$$

and

$$b_{n,\mathrm{wg}}=\frac{1}{n!}\left[n_2\Delta\left(\frac{V}{\bar{\sigma}}\right)^{n-1}\frac{d^n(Vb)}{dV^n}\right]. \quad (13)$$

The group OPD ξ can be written in terms of the first-order dispersion coefficient as

$$\xi=b_1x_1-x_0 \quad (14)$$

and a dispersion function $\psi(s)$ is defined as[9]

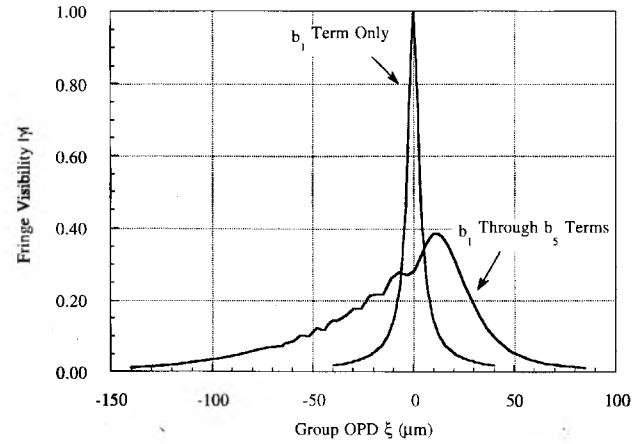

Fig. 2 Plot of fringe visibility versus group OPD. The curves are calculated using the theoretical spectrum for an LED with a mean wavelength of 672 nm, a spectral width of 0.1 μm^{-1}, a fiber length difference of 2 cm, and the dispersion coefficients for silica optical fiber given in Appendix A.

$$\psi(s)=b_2s^2x_1+b_3s^3x_1+b_4s^4x_1+\cdots. \quad (15)$$

Equation (4) can then be written as

$$\sigma X(\sigma)=\bar{\sigma}X(\bar{\sigma})+\xi s+\psi(s). \quad (16)$$

Substituting Eq. (16) into Eq. (2) yields[9] the complex degree of coherence γ as a function of the group OPD ξ:

$$\gamma(\xi)=\exp\left[-j2\pi X(\bar{\sigma})\bar{\sigma}\right]\int_{-\infty}^{\infty}\hat{\mathcal{G}}(s)\exp\left[-j2\pi\psi(s)\right]\times\exp\left(-j2\pi\xi s\right)ds. \quad (17)$$

The term in front of the integral in Eq. (17) represents the oscillatory fringe pattern, while the integral represents the visibility function envelope. Note that this integral is the Fourier transform of $\hat{\mathcal{G}}(s)\exp\left[-j2\pi\psi(s)\right]$.

2.2 *Discussion*

The effects of dispersion in interferometry have been described by Mertz as lowered fringe contrast, broadening of the fringe envelope, and asymmetry introduced into the fringe envelope.[14] These three effects are due to the nature of the dispersion function $\psi(s)$ in Eq. (17). The first-order dispersion coefficient b_1 does not affect the peak value or the shape of the fringe visibility curve. Instead it simply shifts the fringe visibility envelope such that it is centered on zero group OPD. This is apparent from Eq. (17); if we neglect the second and higher order dispersion terms by setting the dispersion function $\psi(s)$ equal to zero, then Eq. (17) is equivalent to the nondispersive Wiener-Khinchin theorem with the OPD X replaced by the group OPD ξ.

As an example of the effects of dispersion, Fig. 2 shows the fringe visibility derived from Eq. (17), using the theoretical spectrum of an LED, which is given by[15]

$$\hat{\mathcal{G}}(\sigma)=\frac{3.6}{\Delta\sigma}\left[\frac{1.8}{\pi\Delta\sigma}\left(\sigma-\bar{\sigma}+\frac{\Delta\sigma}{1.8}\right)\right]^{1/2} \times\exp\left[-\frac{1.8}{\Delta\sigma}\left(\sigma-\bar{\sigma}+\frac{\Delta\sigma}{1.8}\right)\right]. \quad (18)$$

A mean wavelength of 672 nm and a spectral FWHM $\Delta\sigma$ of 0.1 μm^{-1} (corresponding to $\Delta\lambda=45$ nm) were used in the calculations. The two optical fibers were assumed to have a fiber length difference of 2 cm; the dispersion coefficients were calculated for a typical single-mode silica fiber, as described in Appendix A. The first case shown in Fig. 2 includes only the first-order dispersion coefficient b_1. Note that the peak of this curve is unreduced and is located at zero group OPD, as discussed. The second curve includes dispersion terms up to fifth order and illustrates the lowered fringe visibility, envelope broadening, and asymmetry introduced by dispersion.

According to Tango, if the mean wavenumber is chosen correctly using Eq. (3), then the fringe envelope will be centered on the zero of the group OPD ξ and the visibility $|\gamma(0)|$ will be a good approximation to the peak fringe visibility.[9] However, this approximation should be applied with caution because it assumes the visibility curve is symmetric with the peak located near the centroid. As illustrated in Fig. 2, one of the effects of uncompensated dispersion is an asymmetric visibility curve. If the fringe visibility curve is highly asymmetric, it is unlikely that the peak of the curve will coincide with the centroid. If the spectrum is symmetric in wavenumber, then the degree of asymmetry exhibited by the visibility curve will be determined by the ratio of the third-order dispersion coefficient b_3 to the second-order coefficient b_2. However, if the spectrum is asymmetric, then the fringe visibility curve will be asymmetric even if the ratio of b_3/b_2 is small. In either case, the visibility at the centroid of the curve may not give a good estimate of the peak visibility.

2.3 *Calculations of Fringe Visibility for Two Mean Wavelengths*

2.3.1 *Visible wavelength*

To examine the effects of uncompensated dispersion on peak fringe visibility, we calculated the visibility as a function of fiber length difference for the case of a Gaussian (in wavenumber) spectrum with a mean wavelength of 672 nm and a frequency width of 0.04 μm^{-1} (corresponding to $\Delta\lambda=18$ nm). Although narrower than is typically used in stellar interferometry, this spectrum is broad enough to show clearly the effects of dispersion. The dispersion coefficients derived for the Newport F-SPA fiber in Appendix A were used. The fringe visibility was calculated repeatedly using Eq. (17) with the number of terms in $\psi(s)$ increased each time. We found that including terms of higher than fifth order did not affect the calculated visibility appreciably, so a truncation of the Taylor series after the fifth-order term was used in all subsequent calculations. As described, the visibility at zero group OPD may not be the peak visibility, so for each fiber length difference we calculated the visibility for several different values of ξ near zero to search for the peak value, but for this mean wavelength and narrow spectral width, the fringe visibility at zero group OPD was found to be a reasonable approximation to the peak visibility. The result of these calculations is shown as the lower curve in Fig. 3, where it is clear that the fringe visibility drops rapidly as a function of fiber length difference.

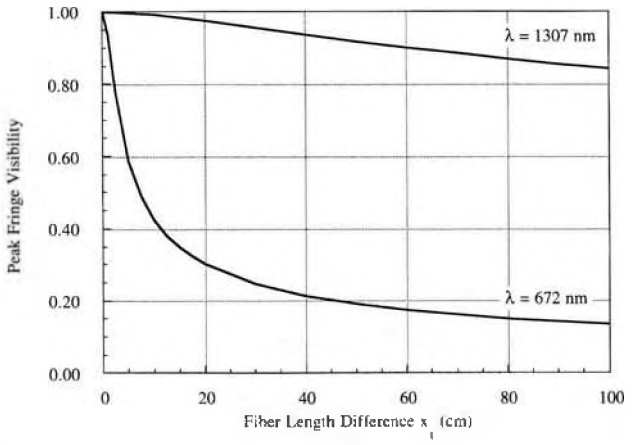

Fig. 3 Plot of the peak fringe visibility versus fiber length difference assuming a Gaussian spectrum centered at either 672 or 1307 nm, each with a FWHM of 0.04 μm^{-1}. The dispersion coefficients are calculated in Appendix A.

2.3.2 *Near IR wavelength*

The fringe visibility can be significantly increased if the dominant dispersion term b_2 is minimized by a judicious choice of operating wavelength. The term b_2 is proportional to the expression for pulse spreading in optical fiber communications, and it is well known that at wavelengths near 1300 nm, the pulse spreading due to material dispersion in silica fibers will cancel that due to waveguide dispersion. We therefore recalculated the peak visibility versus fiber length difference for a Gaussian spectrum with a mean wavelength of 1307 nm and the same frequency width as before (0.04 μm^{-1}, corresponding to $\Delta\lambda=68$ nm). The dispersion coefficients of the Corning fiber (SM.13-P-7/125) from Appendix A were used in the calculation. The zero dispersion wavelength λ_0 of this fiber was calculated to be 1294 nm, but the mean wavelength of our IR laser diode (LD) (1307 nm) is reasonably close to λ_0 and was used for these calculations. At this wavelength, b_2 is near zero and therefore the third and higher order dispersion terms become very important. To find the peak visibility in this case, it is now very important to calculate the visibility as a function of group OPD ξ to identify the peak for each fiber length difference. Tango's finding that the peak fringe visibility lies at $\xi=0$ is based on an approximation of the Taylor series using only the second-order term.[9] If this term is near zero, as here, the higher order terms become more important, and we found that the peak visibility was significantly shifted from zero group OPD. The upper curve in Fig. 3 shows the peak visibility for the spectrum centered at 1307 nm. Note that the peak visibility is significantly improved over the 672 nm case for any given fiber length difference.

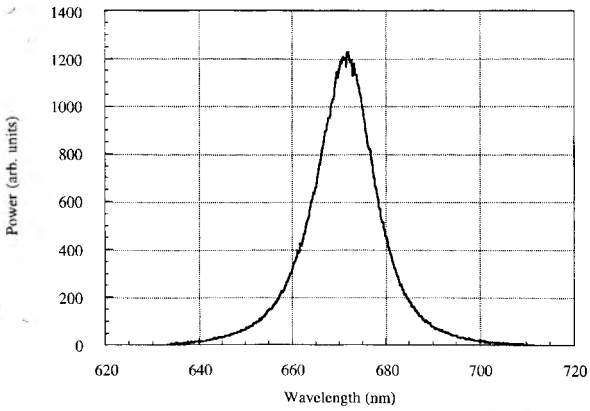

Fig. 4 Spectrum of the Toshiba TOLD 9200 visible LD at 30 mA drive current. This drive current is below the threshold of this LD and this gives a broad spectrum that is useful for characterizing the effects of dispersion.

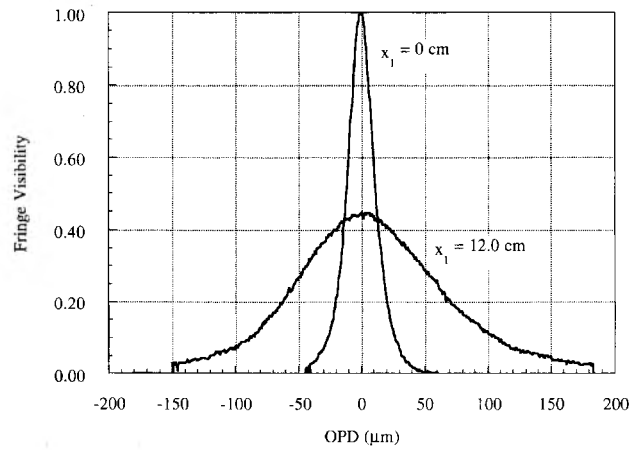

Fig. 5 Plot of the measured fringe visibility curves as a function of the OPD for two different fiber length differences. Both curves are normalized by the corresponding high drive current visibility.

3 Experiment

3.1 *Fringe Visibilities Using a Visible Source*

For the experimental portion of this work, we used a fiber optic Mach-Zehnder interferometer similar to Fig. 1. The source was a Toshiba TOLD 9200 LD with a mean wavelength of 672 nm. LDs are particularly useful for this type of experiment because their coherence length can be varied by changing the drive current.[16] A high drive current can be used for alignment purposes, and then the drive current can be adjusted below threshold to give a broadband source for the actual experiment. The spectrum of this LD at 30 mA drive current, well below threshold, is shown in Fig. 4. This spectrum was measured using a SPEX 1681 spectrograph and a Photometrics CH250 CCD camera.

The fibers were single-mode, PM (SM,PM) fibers (Newport F-SPA). They were initially 3 m long each, and they were matched in physical length to less than 4 mm by gently stretching and cleaving the fibers side by side. The light was coupled to the fibers' input and collimated at their output with 10× microscope objectives.

An LD at low drive current is not spatially coherent, so the two fiber inputs must be carefully superimposed in the plane perpendicular to the incident light to avoid reducing the measured fringe visibility by spatial coherence effects. Recognizing that the output of an SM fiber has nearly perfect spatial coherence, we found that this problem can be eliminated by inserting a short (10 cm) length of SM,PM fiber between the source and the first beamsplitter.

The output end of one of the fibers was mounted on a translation stage driven by a motor micrometer; this enabled us to vary the OPD by varying the air path length of one arm. The light output from the fibers was recombined to form fringes on a Si pin photodiode. The signal from the photodiode was amplified, digitized, and recorded in a computer along with the optical encoder signal from the motor micrometer. The fringe visibility was then calculated from the interferogram data, and the peak visibility was identified. The visibility at high drive current (60 mA) was also measured (typically in the range 0.95 to 0.99) and used to normalize the low-current visibility. The LD spectrum at 60 mA is so narrow that even for large x_1 the fringe visibility is not affected by dispersion. Normalizing eliminates the spurious effects of polarization misalignment, power imbalance, etc.

Fiber 2 was then cleaved by a small amount and the measurement of fringe visibility was repeated. Fiber 2 was initially slightly longer than fiber 1, so we cleaved it in increments of 1 mm and identified the point where the two fibers were equal in optical length from the measured visibilities. This is a more accurate measurement of fiber length difference than a physical comparison, since refractive index variations may cause two fibers that are nominally equal in physical length to be unequal in optical path length.

Typical examples of the fringe visibility as a function of OPD are shown in Fig. 5 for two cases: $x_1 = 0$ cm and $x_1 = 12.0$ cm. These two visibility curves were calculated from the measured interferograms. Both curves were normalized by their corresponding high drive current visibility, as discussed. During the measurements, the interferograms were recorded as a function of relative path length difference; however, the zero absolute path length difference was identified from the peak visibility. As discussed, dispersion may in general shift the peak of the visibility curve from the zero group OPD point, but in this case the ratio of b_2/b_3 is sufficiently high that this shifting of the curves is not expected. The curves in Fig. 5 clearly illustrate the effects of dispersion: the $x_1 = 12.0$ cm case displays lowered fringe visibility and broadening of the interferogram, as well as slight asymmetry.

Figure 6 presents the results of several measurements of the peak fringe visibility as a function of the fiber length imbalance between the two arms. For comparison, a curve calculated using the theory of the previous section is also shown. In calculating the theoretical visibility, the exact spectral shape is very important. We therefore used the measured spectrum of our LD shown in Fig. 4 for these calculations. The spectrum was normalized to give unit area and the fringe visibilities were calculated using Eq. (17) and the dispersion coefficients in Appendix A. As can be seen in Fig. 6, the experimental points matched the theoretical predictions very well.

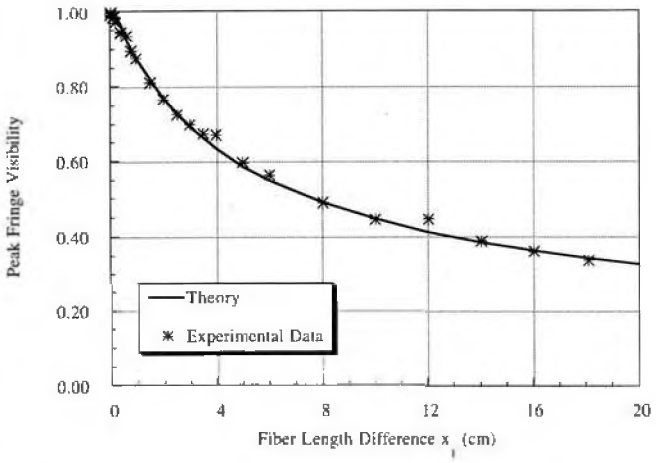

Fig. 6 Comparison of theoretical and measured peak fringe visibility as a function of the fiber length difference x_1 for a source centered at 672 nm. The actual spectrum of the visible LD at 30 mA (Fig. 4) was used to calculate the theoretical curve; this spectrum is approximately 2.5 times narrower than that used to calculate Fig. 2.

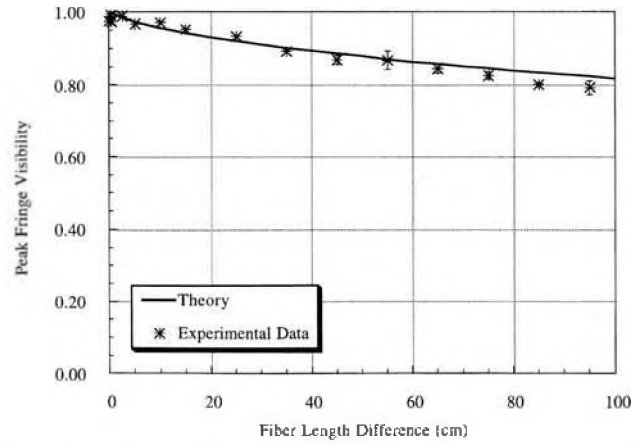

Fig. 8 Comparison of theoretical and measured peak fringe visibility as a function of the fiber length difference x_1 for a source centered at 1307 nm. The actual spectrum of the infrared LD at 1.1 mA (Fig. 7) was used to calculate the theoretical curve. The stars and error bars indicate the mean and standard deviation, respectively, for points where the visibility was measured repeatedly.

3.2 *Fringe Visibilities Using an IR Source*

The IR visibilities were measured using a fiber optic interferometer similar to the one used in the visible experiment. The source was an LD with a mean wavelength of 1307 nm (AT&T x261A Astrotec Laser-Pac). This source had an SM fiber pigtail, which eliminates the need for an extra SM fiber section to ensure spatial coherence. The spectrum at a drive current of 1.1 mA, well below threshold, was measured using an optical spectrum analyzer (HP 70951B), and is shown in Fig. 7.

Two 2.5 m sections of SM.PM fiber (Corning/Fujikura SM.13-P-7/125) were initially cleaved side by side to equal lengths; then one fiber was cleaved to successively shorter lengths, as described earlier. For each fiber length difference, the entire central lobe of the interferogram was recorded to enable identification of the peak visibility. As in the visible case, the low drive current (1.1 mA) visibilities were normalized by the corresponding high drive current (15.5 mA) visibilities. For each fiber length difference the peak visibility was identified from the measured data.

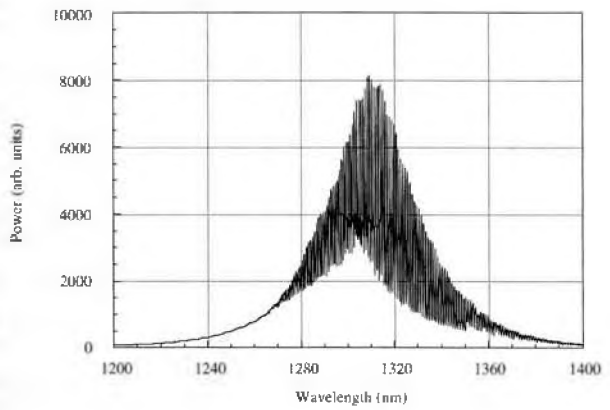

Fig. 7 Spectrum of the AT&T x261A Astrotec Laser-Pac LD at 1.1 mA drive current.

Figure 8 shows the experimental measurements of peak visibility as a function of fiber length difference for 1307 nm illumination. Also shown for comparison is a curve of the theoretical peak visibility calculated from Eq. (17) using the actual LD spectrum (Fig. 7) and the dispersion coefficients of the Corning fiber (Appendix A). Again, there is very good agreement between the theory and experimental measurements.

4 Conclusions

This analysis of dispersion in fiber optic interferometry, including the effects of both material and waveguide dispersion, has shown that dispersion causes the peak fringe visibility to decrease and that it shifts, broadens and in some cases skews the interferogram. The fringe visibility can be significantly improved if wavelengths near 1300 nm are used, due to cancellation of the second-order material and waveguide dispersion terms. The close correlation between the theoretical and experimental data points indicates that the theory provides excellent predictions of actual visibilities, despite the number of approximations made in the analysis.

One important conclusion of this analysis is that optical fibers can be a practical solution to the beam transport problem in stellar interferometry. Although the maximum fiber length difference that can be tolerated depends on the central wavelength and bandwidth, this analysis has demonstrated that, with the appropriate choice of central wavelength, the maximum fiber length difference is on the order of 10 cm (see Fig. 8). Therefore, it is not necessary to precisely match the optical fiber lengths in a practical stellar interferometer. However, it is important to note that optical fibers cannot be used to compensate the full vacuum path difference in a true stellar interferometer. For example, the CHARA interferometer will have a vacuum path difference of the order of 100 m, and this analysis has demonstrated that fiber length differences that large cannot be tolerated. For a long baseline stellar interferometer, the best solution may be a combination of fiber and vacuum or air

Table 1 Dispersion coefficients calculated for Newport and Corning optical fibers.

Dispersion Coefficients	Newport Fiber F-SPA $\lambda = 672$ nm	Corning Fiber SM.13P-7/125 $\lambda = 1307$ nm
$b_{1,mat}$	1.472	1.462
$b_{1,wg}$	0.002463	0.004922
$b_{1,tot}$	1.474	1.467
$b_{2,mat} \times 10^2$	1.350	−0.08425
$b_{2,wg} \times 10^2$	0.1902	0.05524
$b_{2,tot} \times 10^2$	1.540	−0.02901
$b_{3,mat} \times 10^2$	0.4372	1.431
$b_{3,wg} \times 10^2$	−0.08838	−0.1718
$b_{3,tot} \times 10^2$	0.3488	1.259
$b_{4,mat} \times 10^2$	−0.02168	−1.575
$b_{4,wg} \times 10^2$	−0.008724	0.2809
$b_{4,tot} \times 10^2$	−0.03040	−1.294
$b_{5,mat} \times 10^2$	0.03657	2.295
$b_{5,wg} \times 10^2$	0.07239	−0.3618
$b_{5,tot} \times 10^2$	0.1090	1.933

paths. One option that may allow for longer fiber length differences is the addition of dispersion compensators to the system.

In an actual stellar interferometric application, it is the complete mutual coherence, including both spatial and temporal effects, that is of interest for reconstructing both the spectrum and shape of the object. In that case, the power spectral density of the source can be related to the mutual coherence function through a 3D Fourier transform, which consists of a 2D spatial transform and a 1D temporal transform. This is often referred to as double Fourier interferometry,[17,18] and will be the topic of a following paper. The effects of dispersion in double Fourier interferometry can be predicted from the analysis described here. The spatial transform will be unaffected by dispersion, and the expressions derived here can be applied directly to the dispersive temporal transform.

5 Appendix A

5.1 *Calculation of Material Dispersion Coefficients*

Most SM fibers for visible and near-IR wavelengths are made of silica-based glasses. The cores of both the Newport and Corning fibers used in this experiment were made of SiO_2 lightly doped with GeO_2 (germania), and the claddings were pure SiO_2. The refractive index as a function of wavelength was calculated from the Sellmeier equation for fused silica.[19] The material dispersion coefficients were obtained from Eq. (12), with the derivatives of the refractive index calculated symbolically using Mathematica. The material dispersion coefficients for the Newport F-SPA fiber at a wavelength of 672 nm and for the Corning fiber at a wavelength of 1307 nm are shown in Table 1.

In the experimental portion of this work, the fiber length difference was balanced by adding an extra air path in the opposite arm of the interferometer. This air path is dispersive, and this should theoretically be taken into account in the calculations. The material dispersion coefficients of this air path at wavelengths of 672 and 1307 nm were calculated from Eq. (12) using the refractive index formula for air[20] (assuming a relative humidity of 50%, and $T = 297$ K), but we found that even at IR wavelengths the dispersion of air is so small compared to the dispersion of fibers that it can be neglected.

5.2 *Calculation of Waveguide Dispersion Coefficients*

The waveguide dispersion coefficients were calculated from Eq. (13), which requires the Δ and V parameters for the fiber. The values of Δ, numerical aperture (NA) and mode field diameter (MFD) were obtained from the manufacturers' specifications, but for the case of the Corning fiber we measured the MFD using a transverse offset method,[21] and found an MFD of 10.7 μm.

When calculating the waveguide dispersion coefficients, the method used to calculate $d^2(Vb)/dV^2$ is very important. The method of Huang and Wang[22] gives an error smaller than 4% for $1.2 < V < 3$ (Ref. 23), and the waveguide dispersion coefficients were calculated using this method, with higher order derivatives of Vb calculated symbolically using Mathematica. The waveguide dispersion coefficients and the total dispersion coefficients of both the Newport fiber and the Corning fiber are given in Table 1.

Acknowledgments

This work was sponsored in part by the U.S. Air Force Office of Scientific Research. Gary Loos, Michael McNeely, Sergio Restaino, Stuart Shaklan, and Zhao Peiqian provided helpful discussions. S. Dyer gratefully acknowledges the support of a Patricia Harris Fellowship and a University of Utah Fellowship. The IR LD was provided by AT&T Bell Laboratories.

References

1. W. J. Tango and R. Q. Twiss, "Michelson Stellar Interferometry," *Prog. Opt.* **17**, 240–277 (1980).
2. J. W. Goodman, *Statistical Optics*, John Wiley & Sons, New York (1985).
3. H. A. McAlister, W. G. Banuolo, T. A. ten Brummelaar, W. I. Hartkopf, N. H. Turner, A. K. Garrison, W. G. Robinson, and S. T. Ridgway, "The CHARA array," in *Amplitude and Intensity Spatial Interferometry II*, J. B. Breckinridge, Ed., *Proc. SPIE* **2200**, 129–139 (1994).
4. C. Froehly, "Coherence and Interferometry through optical fibers," in *Proc. ESO Conf. on Scientific Importance of High Angular Resolution at Infrared and Optical Wavelengths*, M. H. Ulrich, Ed., Garching, Germany, pp. 285–293 (1981).
5. S. B. Shaklan and F. Roddier, "Single-mode fiber optics in a long-baseline interferometer," *Appl. Opt.* **26**, 2159–2163 (1987).
6. S. B. Shaklan, "Multiple beam correlation using single-mode fiber optics with application to interferometric imaging," PhD Dissertation, University of Arizona (1989).
7. S. B. Shaklan, "Fiber optic beam combiner for multiple-telescope interferometry," *Opt. Eng.* **29**, 684–689 (1990).
8. J. J. Alleman, F. Reynaud, and P. Connes, "Fiber-linked telescope array: description and laboratory tests of a two-channel prototype," *Appl. Opt.* **34**, 2284–2294 (1995).
9. W. J. Tango, "Dispersion in stellar interferometry," *Appl. Opt.* **29**, 516–521 (1990).
10. F. Reynaud, J. J. Alleman, and P. Connes, "Interferometric control of fiber lengths for a coherent telescope array," *Appl. Opt.* **31**, 3736–3743 (1992).
11. V. Coudé du Foresto, G. Perrin, and M. Boccas, "Minimization of fiber dispersion effects in double Fourier stellar interferometers," *Astron. Astrophys.* **293**, 278–286 (1995).
12. G. Keiser, *Optical Fiber Communications*, McGraw-Hill. New York (1983).

13. D. Gloge, "Weakly guiding fibers," *Appl. Opt.* **10**, 2252–2258 (1971).
14. L. Mertz, *Transformations in Optics*, John Wiley & Sons, New York (1965).
15. B. Saleh and M. Teich, *Fundamentals of Photonics*, John Wiley & Sons, New York (1991).
16. D. A. Christensen, J. Rotgé, A. Klemas, G. Loos, and D. Merriman, "Laser diode coherence length variation for balancing fiber optic interferometers," *Opt. Eng.* **33**, 2034–2038 (1994).
17. J.-M. Mariotti and S. T. Ridgway, "Double Fourier spatio-spectral interferometry: combining high spectral and high spatial resolution in the near infrared," *Astron. Astrophys.* **195**, 350–363 (1988).
18. P. Zhao, J.-M. Mariotti, P. Léna, V. Coudé du Foresto, and B. Zhou, "Double Fourier interferometry with IR single-mode fiber optics," *Opt. Commun.* **110**, 497–502 (1994).
19. W. L. Wolfe, "Properties of optical materials," in *Handbook of Optics*, W. G. Driscoll and W. Vaughn, Eds., Mc-Graw Hill, New York (1978).
20. J. C. Owens, "Optical refractive index of air: dependence on pressure, temperature and composition," *Appl. Opt.* **6**, 51–59 (1967).
21. W. T. Anderson, "Consistency of measurement methods for the mode field radius in a single-mode fiber," *IEEE J. Lightwave Technol.* **LT-2**, 191–197 (1984).
22. H.-C. Huang and Z.-H. Wang, "Analytical approach to prediction of dispersion properties of step-index single mode optical fibers," *Electron. Lett.* **17**, 202–204 (1981).
23. L. B. Jeunhomme, *Single-Mode Fiber Optics*, Marcel Dekker, New York (1990).

Shellee D. Dyer received her PhD in electrical engineering from the University of Utah in 1996. Since then she has been doing her postdoctoral research at the National Institute of Standards and Technology in Boulder, Colorado. Her current research interests include erbium fiber superfluorescent sources and low-coherence fiber optic sensors.

Douglas A. Christensen received the BSEE degree from Brigham Young University in 1962, the MS degree from Stanford University in 1963, and the PhD degree from the University of Utah in 1967. During 1972–74, he held a special NIH postdoctorate position in biomedical engineering at the University of Washington. He has been a faculty member at the University of Utah since 1971. He currently holds a joint appointment as professor of electrical engineering and professor of bioengineering. His major research interests are in the area of waves in biological sensing, including optical biosensors, fluorescent waveguiding immunosensors, numerical modeling of optical waveguides and near-field optical effects, and ultrasonic bioinstrumentation. He is the author of the textbook *Ultrasonic Bioinstrumentation*, published by Wiley in 1988.